

# Vanadium Oxides on Aluminum Oxide Supports. 1. Surface Termination and Reducibility of Vanadia Films on $\alpha$ -Al<sub>2</sub>O<sub>3</sub>(0001)

Tanya K. Todorova,<sup>†</sup> M. Veronica Ganduglia-Pirovano,\* and Joachim Sauer

Humboldt-Universität zu Berlin, Institut für Chemie, Unter den Linden 6, D-10099 Berlin, Germany

Received: July 15, 2005; In Final Form: September 30, 2005

Using density functional theory and statistical thermodynamics, we obtained the phase diagram of thin V<sub>n</sub>O<sub>m</sub> films of varying thickness ( $\sim 2$ – $6$  Å, 1–6 vanadium layers) supported on  $\alpha$ -Al<sub>2</sub>O<sub>3</sub>(0001). Depending on the temperature, oxygen pressure, and vanadium concentration, films with different thickness and termination may form. In ultrahigh vacuum (UHV), at room temperature and for low vanadium concentrations, an ultrathin (1  $\times$  1) O=V-terminated film is most stable. As more vanadium is supplied, the thickest possible films form. Their structures and terminations correspond to previous findings for the (0001) surface of bulk V<sub>2</sub>O<sub>3</sub> [Kresse et al., *Surf. Sci.* **2004**, 555, 118]. The presence of surface vanadyl (O=V) groups is a prevalent feature. They are stable up to at least 800 K in UHV. Vanadyl oxygen atoms induce a V<sub>2p</sub> core-level shift of about 2 eV on the surface V atoms. The reducibility of the supported films is characterized by the energy of oxygen defect formation. For the stable structures, the results vary between 4.11 and 3.59 eV per 1/2O<sub>2</sub>. In contrast, oxygen removal from the V<sub>2</sub>O<sub>5</sub>(001) surface is much easier (1.93 eV). This provides a possible explanation for the lower catalytic activity of vanadium oxides supported on alumina compared to that of crystalline vanadia particles.

## I. Introduction

Submonolayer to monolayer quantities of vanadia supported on oxides such as Al<sub>2</sub>O<sub>3</sub>, SiO<sub>2</sub>, TiO<sub>2</sub>, or ZrO<sub>2</sub> are known to be active catalysts for a variety of industrially applied oxidation reactions. The oxidation involves Mars–van Krevelen redox cycles with lattice oxygen as the reactive intermediates.<sup>1</sup> Mechanistic studies have shown that reduced V centers (V<sup>III</sup> or V<sup>IV</sup>) are present at low concentrations during steady-state catalysis and that the extent of reduction correlates with turnover frequencies.<sup>2</sup> Moreover, the performance of supported vanadia catalysts also depends on the oxide support.<sup>3,4</sup> Yet, the nature of the active surface and the role of the supporting oxide are far from being known. The reason is the complex structure of the real catalysts and the effect of the ambient environment. However, this knowledge is essential for the rational design of active and selective supported vanadia catalysts in many redox reactions. A better understanding of the catalytic properties requires a determination of the structure–reactivity relationships of the supported VO<sub>x</sub> catalysts. Theoretical and experimental studies on well-defined model catalysts, such as vanadia particles and films of varying thickness supported on different oxides, are necessary to build up this knowledge. The vanadia/TiO<sub>2</sub> system has received much attention,<sup>5–9</sup> and recent studies have considered the vanadia/Al<sub>2</sub>O<sub>3</sub> system as well.<sup>10–15</sup>

The experimental vanadia/alumina model catalyst, prepared via evaporation of vanadium onto a thin alumina film in ultrahigh vacuum (UHV), consists of vanadia particles (20–30 Å wide, 3–6 Å thick) with vanadium in an average oxidation state III.<sup>10</sup> Using infrared (IR) spectroscopy, surface vanadyl groups (O=V) have been identified, which are not structural elements of bulk truncated V<sub>2</sub>O<sub>3</sub> surfaces. Evidence for the

vanadyl termination of well-ordered V<sub>2</sub>O<sub>3</sub>(0001) films has recently been produced by high-resolution electron energy loss spectroscopy (HREELS) and surface-sensitive X-ray photoelectron spectroscopy (XPS) studies.<sup>16</sup> For epitaxially grown V<sub>2</sub>O<sub>3</sub> films on Pd(111) and Rh(111), Surnev et al.<sup>17–20</sup> and Schoiswohl et al.<sup>21,22</sup> observed different terminations depending on the growth conditions and film thickness that include terminal vanadyl (O=V) species. In contrast, on Cu<sub>3</sub>Au(100), Niehus et al.<sup>23,24</sup> did not find evidence of O=V termination.

The structure and vibrational properties of a V<sub>2</sub>O<sub>3</sub> monolayer film supported on  $\alpha$ -Al<sub>2</sub>O<sub>3</sub>(0001) have recently been theoretically investigated.<sup>13</sup> Oxygen adsorption on its surface vanadium sites results in strongly bound O=V species with (1  $\times$  1) periodicity. The O=V stretch frequencies are similar to those on the V<sub>2</sub>O<sub>5</sub>(001) single-crystal surface, which is in agreement with the experimental observations for vanadia particles on alumina.<sup>10</sup> In this study, we further investigate the geometrical and electronic properties of V<sub>2</sub>O<sub>3</sub> films on  $\alpha$ -Al<sub>2</sub>O<sub>3</sub>(0001) surfaces using density functional theory (DFT) combined with statistical thermodynamics. The stability of films with varying thickness of up to  $\sim 6$  Å and different terminations is examined as a function of the oxygen partial pressure and the vanadium concentration at finite temperature. The resulting phase diagram shows that different terminations may prevail depending on the film thickness and that the presence of vanadyl (O=V) groups is a dominant feature. The stable terminations of thick films are those predicted by Kresse et al.<sup>25</sup> for the crystalline V<sub>2</sub>O<sub>3</sub>(0001) surface, which have also been recently observed.<sup>22</sup>

With respect to reactivity, we discuss the surface reducibility (i.e., the energy of O-defect formation) as a function of the film thickness and defect concentration. Oxygen is most easily removed from the vanadyl groups, and we show that the strength of the O=V bond may vary up to  $\sim 0.5$  eV/atom. Hence, different conditions may significantly affect the surface reducibility.

\* To whom correspondence should be addressed. E-mail: vgp@chemie.hu-berlin.de

<sup>†</sup> Member of the International Max Planck Research School “Complex Surfaces in Material Science”.

**TABLE 1: Lattice Constants (Å) for the Hexagonal Bulk Al<sub>2</sub>O<sub>3</sub> and V<sub>2</sub>O<sub>3</sub> Structures**

		$a_{\text{hex}}$	$c_{\text{hex}}$
Al <sub>2</sub> O <sub>3</sub>	exptl <sup>a</sup>	4.757	12.988
	this work	4.804	13.107
V <sub>2</sub> O <sub>3</sub>	exptl <sup>b</sup>	4.940	13.971
	this work	4.856	14.349

<sup>a</sup> Ref 53. <sup>b</sup> Ref 54.

## II. Methods and Models

**A. Computational Details.** The present spin-polarized DFT calculations apply periodic boundary conditions and employ a plane-wave basis set as implemented in the Vienna ab initio simulation package (VASP).<sup>26–29</sup> The generalized gradient-corrected functional of Perdew and Wang (PW91)<sup>30</sup> is used. The electron–ion interaction is described by the projector augmented wave (PAW) method.<sup>31,32</sup> Core radii of 2.3 and 1.9 au are used for V and Al, respectively. For oxygen, the core radii are 1.2 and 1.52 au for the s and p states, respectively. The 3p states of vanadium are treated as valence states to guarantee good transferability of the vanadium potential. A plane-wave basis set up to a kinetic energy of 800 eV is used. The Brillouin-zone (BZ) integration employs the Monkhorst–Pack technique.<sup>33</sup>

The corundum structure of  $\alpha$ -Al<sub>2</sub>O<sub>3</sub> belongs to the space group R $\bar{3}c$ . The lattice parameters of the rhombohedral cell and fractional coordinates were simultaneously optimized using a (3 × 3 × 3)  $k$  mesh. The parameters of the corresponding hexagonal cell are listed in Table 1.

The accuracy of the present cutoff and  $k$ -points mesh is judged on calculations that use a denser  $k$ -point grid (4 × 4 × 4) and a higher cutoff (1200 eV). The corresponding changes of the optimized cell parameters are smaller than 0.001 Å. Thus, the 800 eV cutoff and a (3 × 3 × 3)  $k$  mesh are used for calculations on a slab of six trilayers of the Al<sub>2</sub>O<sub>3</sub>(0001) surface. Each of the six (Al–O<sub>3</sub>–Al) trilayers maintains the bulk composition. A vacuum region of  $\sim 10$  Å is used to decouple the surfaces of consecutive slabs in the supercell. A (3 × 3 × 1)  $k$ -point grid that includes the  $\bar{\Gamma}$  point is used for the (1 × 1) hexagonal surface unit cell. The position of all ions is relaxed by a conjugate-gradient algorithm until the forces are smaller than 1 meV/Å. The interlayer spacings are in very good agreement with previous DFT studies<sup>34–36</sup> and confirm the large inward relaxation (86%) of the outermost Al layer.

To evaluate the O-defect formation energies (see section III.D), the total energy of the isolated oxygen molecule is needed. A (13 × 14 × 15) Å<sup>3</sup> orthorhombic unit cell with  $\Gamma$ -point sampling of the BZ is used. The binding energy per O atom in O<sub>2</sub> is 3.14 eV/atom, and the bond distance is 1.222 Å. The experimental result is 2.59 eV/atom (obtained after adding the contributions due to zero-point vibrations to the  $T = 0$  K value) and 1.207 Å, respectively.<sup>37</sup> The overestimation of the binding energy and the bond distance are in line with earlier density functional calculations that used gradient-corrected functionals<sup>38,39</sup> (see also ref 40 for a comparison of different functionals).

**B. Supported Vanadium Oxide Films.** One possible way to model vanadium oxides supported on  $\alpha$ -Al<sub>2</sub>O<sub>3</sub>(0001) is to replace the Al atoms by V atoms in subsequent layers of the corundum structure, thereby creating thin V<sub>2</sub>O<sub>3</sub> films on the Al<sub>2</sub>O<sub>3</sub> surface. When terminated by a *single-metal* (V) layer, the unit cell compositions of these slab models obey the general formula  $n/2V_2O_3 \cdot (12 - n)/2Al_2O_3$  ( $n = 1-6, 12$ ). In ref 13,

such models were studied with V atoms in one or two metal layers only ( $n = 1, 2$ ). In this work, we systematically increase the thickness of the vanadium oxide films up to six metal layers. Decreasing the thickness of the Al<sub>2</sub>O<sub>3</sub> support while increasing that of the V<sub>2</sub>O<sub>3</sub> film does not affect the results. The thinnest support still consists of three trilayers. Moreover, the properties of the clean Al<sub>2</sub>O<sub>3</sub>(0001) surface do not change when passing from a three- to a four-trilayer-thick slab (e.g., the surface energy changes by 0.09 J/m<sup>2</sup>).<sup>13</sup> We have also considered the limiting case of replacing Al atoms in all twelve metal layers of the alumina slab. The latter is called a *V<sub>2</sub>O<sub>3</sub>-like* slab because the surface unit cell has the lattice parameters of the  $\alpha$ -Al<sub>2</sub>O<sub>3</sub> support.

The lattice mismatch between the V<sub>2</sub>O<sub>3</sub> and Al<sub>2</sub>O<sub>3</sub> corundum structures is  $\sim 4\%$  in the (0001) plane (see Table 1). By adding an oxygen atom to every vanadium site in the surface layer, (1 × 1) vanadyl terminated films can be created, with the composition  $1/2V_2O_5 \cdot (n - 1)/2V_2O_3 \cdot (12 - n)/2Al_2O_3$  (e.g., see Figure 1D). The composition of the surface layer is V<sub>2</sub>O<sub>5</sub>, but the coordination of vanadium is different from that in the single-crystal V<sub>2</sub>O<sub>5</sub>(001) surface.

Figure 1A shows the supported 6V-layer V<sub>2</sub>O<sub>3</sub> film that is terminated by a single-metal layer, keeping the V<sub>2</sub>O<sub>3</sub> composition. It is named V–O<sub>3</sub>–V(V–O<sub>3</sub>–V) according to the sequence of the V and O atomic layers of the corundum structure from the surface into the bulk. This nomenclature includes only the atomic layers that are relevant for the following discussion, that is, those in the two outermost V–O<sub>3</sub>–V trilayers. The oxygen-terminated O<sub>3</sub>–V(V–O<sub>3</sub>–V) film (Figure 1B, a total of five V layers) and the double-metal-terminated V(V–O<sub>3</sub>–V) film (Figure 1C, also five V layers), together with the single-metal film, belong to the so-called *intrinsic* bulk terminations. They result from the successive removal of the outermost V and O<sub>3</sub> layers, respectively, from the stoichiometric slab. Thus, they do not have V<sub>2</sub>O<sub>3</sub> composition.

Starting from the 6V-layer film, several modifications were considered that include the (1 × 1) vanadyl-terminated film, O=V–O<sub>3</sub>–V(V–O<sub>3</sub>–V) (see Figure 1D). To obtain intermediate situations between a (1 × 1) V-terminated surface ( $\Theta_O = 0$ , in which  $\Theta_O$  is the concentration of vanadyl oxygen atoms) and a (1 × 1) O=V-terminated surface ( $\Theta_O = 1$ ), oxygen atoms were added to 1/4, 1/2, or 3/4 of the vanadium surface sites. Therefore, (2 × 2) unit cells with mixed O=V and V terminations were considered. On the basis of the ( $\sqrt{3} \times \sqrt{3}$ )R30° geometry, two additional oxygen coverages are possible, namely,  $\Theta_O = 1/3$  and  $2/3$  (see Figure 2).

The polar (oxygen-terminated) O<sub>3</sub>–V(V–O<sub>3</sub>–V) surface can *reconstruct* to reduce its polarity. Figure 1E shows one example in which half of the vanadium atoms of the second V double layer pop into the first V double layer, leading to a O<sub>3</sub>–V<sub>3</sub>–O<sub>3</sub> sequence. This corresponds to a nonpolar hexagonal film of VO<sub>2</sub> composition [(VO<sub>2</sub>)<sub>3</sub>] on top of a single V-layer-terminated slab (V–O<sub>3</sub>–V–Al...). This reconstruction has recently been proposed for the (0001) surface of bulk V<sub>2</sub>O<sub>3</sub>.<sup>25</sup> Another way of reducing the polarity is to remove 1/3 or 2/3 of the oxygen atoms from the O<sub>3</sub> surface layer, creating surface terminations with 2/3 (Figure 1F) and 1/3 (Figure 1G) monolayers (MLs) of O atoms at bridge positions. Their electronic and structural properties have recently been theoretically investigated for the V<sub>2</sub>O<sub>3</sub>(0001) surface using cluster models.<sup>41</sup> The O<sub>2</sub><sup>b</sup>(V–O<sub>3</sub>–V) termination (Figure 1F) corresponds to the structural model of refs 23 and 24 for the termination of the V<sub>2</sub>O<sub>3</sub>/Cu<sub>3</sub>Au(100) film. An even more V-rich surface termination can be created from the double-metal-terminated film (Figure 1C) by fully occupying

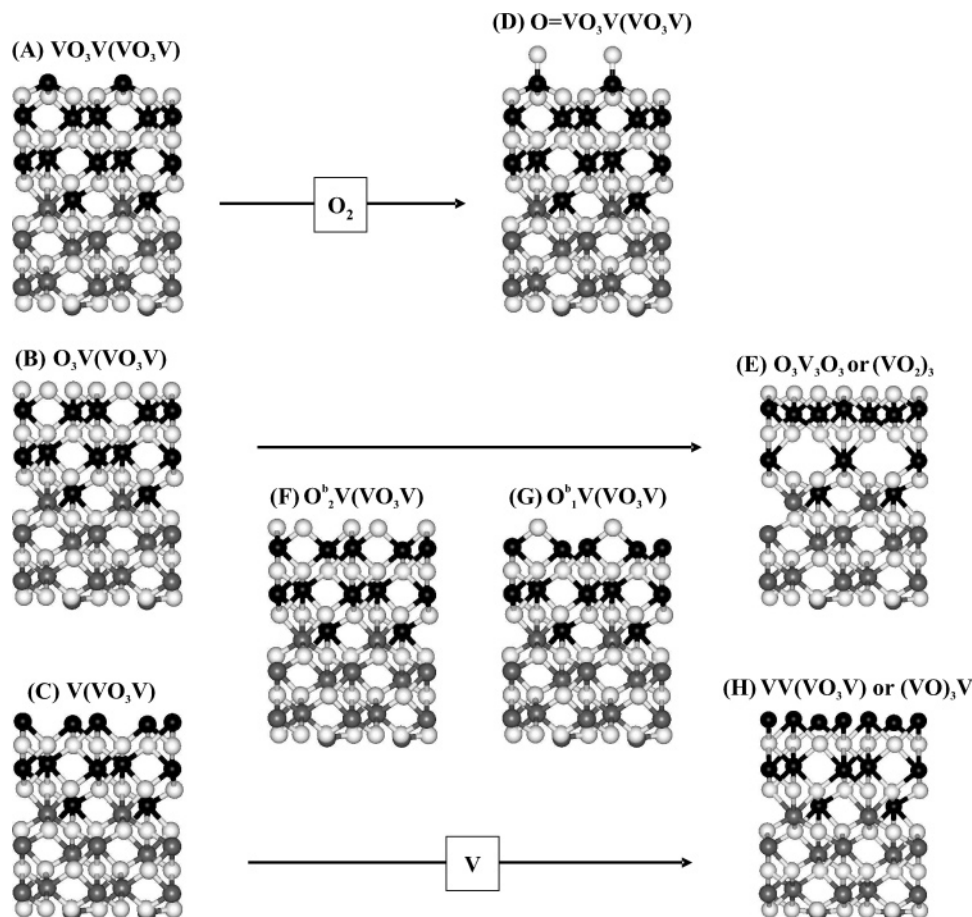


**Figure 1.** Side view of the models for differently terminated 6V-layer-supported oxide films with  $(1 \times 1)$  periodicity. The models are labeled according to the sequence of atomic layers from the surface into the bulk (see Sec. 2.2). The nomenclature includes only the two outermost (V–O<sub>3</sub>–V) trilayers. (A) V–O<sub>3</sub>–V(V–O<sub>3</sub>–V), (B) O<sub>3</sub>–V(V–O<sub>3</sub>–V), (C) V(V–O<sub>3</sub>–V), (D) O=V–O<sub>3</sub>–V(V–O<sub>3</sub>–V), (E) O<sub>3</sub>–V<sub>3</sub>–O<sub>3</sub>, (F) O<sup>b</sup><sub>2</sub>–V(V–O<sub>3</sub>–V), (G) O<sup>b</sup><sub>1</sub>–V(V–O<sub>3</sub>–V), and (H) VV(V–O<sub>3</sub>–V). Vanadium atoms are black, aluminum atoms are gray, and oxygen atoms are white.

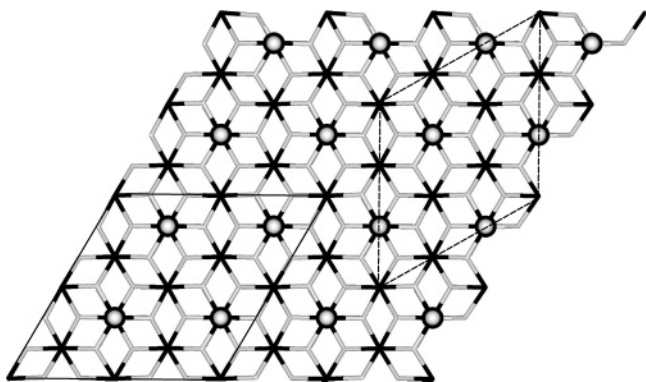


**Figure 2.** Top view of a fully O=V-covered surface of a V<sub>2</sub>O<sub>3</sub> film supported on  $\alpha$ -Al<sub>2</sub>O<sub>3</sub>.  $(2 \times 2)$  and  $(\sqrt{3} \times \sqrt{3})R30^\circ$  unit cells are indicated by solid and broken lines, respectively.

the topmost layer with V atoms, yielding VV(V–O<sub>3</sub>–V) or (VO)<sub>3</sub>V (Figure 1H).

The O<sub>3</sub>–V<sub>3</sub>–O<sub>3</sub> surface (Figure 1E) discussed above can also be obtained from a fully vanadyl-covered film by removing all of the O=V groups and subsequent reconstruction. Moreover, we consider surfaces with a  $(\sqrt{3} \times \sqrt{3})R30^\circ$  periodicity, in which only part of the vanadyl groups (1/3 or 2/3) is removed and the above-described reconstruction is made, except for the sites with O=V groups. Their terminations are given by the

following general formula: (O=V)<sub>x</sub>–O<sub>3</sub>–V<sub>3–x</sub>–O<sub>3</sub>–V<sub>x</sub>, with  $x = 1/3$  and  $2/3$  being the concentration of the O=V groups. In the following sections, they will be termed  $\sqrt{3}$ –(O=V)<sub>x</sub> films. The three reconstructed structures are investigated for two film thicknesses, namely, 4V and 6V layers. Removal of single vanadyl oxygen atoms from these surfaces was also considered, and the corresponding surfaces are labeled  $\sqrt{3}$ –(O=V<sup>reduced</sup>)<sub>x</sub>.

The unit cell compositions of all structures investigated are listed in the Supporting Information.

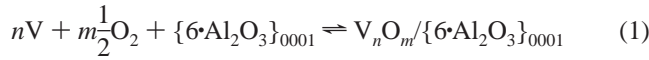
To sample the surface BZ of the vanadia/ $\alpha$ -alumina systems, a  $(6 \times 6 \times 1)$  *k* mesh for the  $(1 \times 1)$  hexagonal cell was used. The larger mesh, compared to the  $(3 \times 3 \times 1)$  grid used for the alumina support (cf. section II.A), is required because of the metallic character of V<sub>2</sub>O<sub>3</sub>. For the larger  $(2 \times 1)$ ,  $(\sqrt{3} \times \sqrt{3})R30^\circ$  and  $(2 \times 2)$  surface unit cells,  $(3 \times 6 \times 1)$ ,  $(3 \times 3 \times 1)$ , and  $(3 \times 3 \times 1)$  grids were used, respectively.

### III. Results and Discussions

**A. Thermodynamic Stability of Alumina-Supported Vanadia Films.** We use statistical thermodynamics to take into account the effects of vanadium activity (or concentration) and oxygen partial pressure at a given temperature on the stability of alumina-supported vanadia films. This strategy has previously been applied to a wide range of problems that involve varying chemical compositions (e.g., see refs 35, 42, and 43).

Typically, supported vanadium oxide films are prepared by evaporating metallic vanadium on the support in an oxygen

atmosphere. Thus, we consider the following equilibrium reaction:



with the energy change

$$\Delta E = \left[ E^{V_nO_m/\{6\cdot Al_2O_3\}_{0001}} - E^{\{6\cdot Al_2O_3\}_{0001}} - nE_V^{bulk} - m\frac{1}{2}E_{O_2} \right] \quad (2)$$

Here,  $E^{V_nO_m/\{6\cdot Al_2O_3\}_{0001}}$  and  $E^{\{6\cdot Al_2O_3\}_{0001}}$  are the total energies of the slab with a given composition and surface termination and the six trilayer  $\alpha$ - $Al_2O_3$  slab, respectively. Note that the energies always refer to slabs with the same amount of  $Al_2O_3$ , namely, 6 formula units (see also Supporting Information).  $E_V^{bulk}$  and  $E_{O_2}$  are the total energies of metallic bcc bulk vanadium and the free oxygen molecule, respectively. The accompanying change in the surface free energy  $\Delta\gamma$  is

$$\Delta\gamma(T, p) = \frac{1}{A}[\Delta E - n\Delta\mu_V - m\Delta\mu_O] \quad (3)$$

Here we introduce chemical potential differences,  $\Delta\mu_i$ , as

$$\Delta\mu_V(T, a_V) = \mu_V(T, a_V) - E_V^{bulk} \quad (4)$$

$$\Delta\mu_O(T, p) = \frac{1}{2}[\mu_{O_2}(T, p) - E_{O_2}] \quad (5)$$

The Gibbs free energies of the solid components are approximated by the energies calculated using DFT. This means that zero-point vibrations, vibrational entropy contributions, and enthalpy changes are neglected.  $A$  is the area of the surface unit cell,  $\mu_i$  ( $i = V$  and  $O$ ),  $n$ , and  $m$  are the chemical potential and the number of  $V$  and  $O$  atoms in the supported vanadia film, respectively. It is assumed that the number of  $V$  and  $O$  atoms removed or added to the slab varies independently. Thus, two independent extensive thermodynamic variables,  $\mu_V$  and  $\mu_{O_2}$ , control the film formation. It is understood that the  $V$  and  $O$  particle reservoirs are in equilibrium with bulk  $V$  and  $O_2$  in the gas phase.

The  $V$  and  $O$  chemical potentials depend on the temperature and the vanadium activity,  $a_V$  (in reference to the corresponding crystalline solid), or the oxygen partial pressure,  $p$  (in reference to the molecular gas), respectively. As the surrounding  $O_2$  atmosphere forms an ideal gas reservoir, the pressure dependence of  $\Delta\mu_O(T, p)$  at a given temperature is given by

$$\Delta\mu_O(T, p) = \frac{1}{2}[H(T, p^\circ) - H(0\text{ K}, p^\circ) - TS(T, p^\circ) + RT \ln(p/p^\circ)] \quad (6)$$

using  $\mu_{O_2}(0\text{ K}) = E_{O_2}$ . Here,  $p^\circ$  is the pressure of the reference state ( $p^\circ = 1\text{ atm}$ ). For a solid component,  $\Delta\mu_V(T, a_V)$  is given by

$$\Delta\mu_V(T, a_V) = \Delta\mu_V(T_r) + \left[ \int_{T_r}^T C_p dT - (T - T_r)S^\circ(T_r) - T \int_{T_r}^T (C_p/T) dT \right] + RT \ln(a_V) \quad (7)$$

with

$$\Delta\mu_V(T_r) = H^\circ(T_r) - H^\circ(0\text{ K}) - T_r S^\circ(T_r) \quad (8)$$

Here,  $\mu_V(0\text{ K}) = E_V^{bulk}$  has been used.  $T_r = 298.15\text{ K}$  and

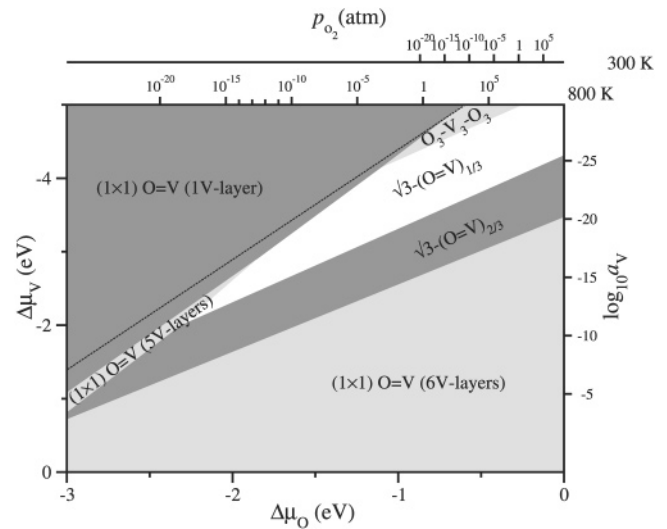


**Figure 3.** Phase diagram as a function of the  $\Delta\mu_O$  and  $\Delta\mu_V$  chemical potentials for alumina-supported thin  $V_nO_m$  films. The  $O_3-V_3-O_3$  film has 5V layers (Figure 1E), and the reconstructed  $\sqrt{3}-(O=V)_x$  terminations are those derive from the  $(1 \times 1)$   $O=V$  6V-layer film (see section 2.2).  $\Delta\mu_O$  and  $\Delta\mu_V$  have been translated into a pressure scale at  $T = 300$  and  $800\text{ K}$  and an activity scale at  $T = 800\text{ K}$ , respectively. The values of  $\Delta\mu_V$  and  $\Delta\mu_O$  that would correspond to  $V$  and  $O$  reservoirs in thermodynamic equilibrium with the  $V_2O_3$  bulk phase are indicated by a dotted line (see section III.A).

tabulated values for the enthalpy  $H$ , entropy  $S$ , and given expressions for the temperature dependence of the specific heat  $C_p(T)$  are used.<sup>44–46</sup> From a practical point of view, the vanadium activity can be varied by controlling the amount of evaporated vanadium forming the oxide film and is related to the concentration through the activity coefficient,  $\gamma_V$ .<sup>47</sup>

To determine the most stable surface for a given set of chemical potentials ( $\Delta\mu_O$  and  $\Delta\mu_V$ ), the surface free energy is calculated for *all* systems investigated. The one with the lowest  $\Delta\gamma$  is the thermodynamically stable phase for the corresponding conditions. The resulting two-dimensional (2D)-surface phase diagram is shown in Figure 3 (see also Supporting Information). The two axes correspond to the chemical potentials  $\Delta\mu_O$  and  $\Delta\mu_V$ .

The former is translated into an oxygen pressure scale for the example of  $T = 300$  and  $800\text{ K}$ , using eq 6 (see the upper axis in Figure 3).

If the  $V$  and  $O$  particle reservoirs would be in thermodynamic equilibrium with vanadia bulk phases, for example,  $V_2O_3$  or  $VO_2$ , the vanadium and oxygen chemical potentials will be coupled by

$$2\Delta\mu_V + 3\Delta\mu_O = \Delta E^{V_2O_3} \quad (9)$$

or

$$\Delta\mu_V + 2\Delta\mu_O = \Delta E^{VO_2} \quad (10)$$

respectively. A plot of eq 9 is shown in Figure 3.  $\Delta E^{V_2O_3}$  and  $\Delta E^{VO_2}$  are the energies of formation of the bulk oxides:

$$\Delta E^{V_2O_3} = E_{V_2O_3}^{bulk} - 2E_V^{bulk} - \frac{3}{2}E_{O_2} \quad (11)$$

$$\Delta E^{VO_2} = E_{VO_2}^{bulk} - E_V^{bulk} - E_{O_2} \quad (12)$$

for which our DFT calculations give  $-11.78$  ( $V_2O_3$ ) and  $-7.24$  ( $VO_2$ ) eV/per formula unit. The experimental results for the heat

of formation at 298.15 K are  $-12.63$  and  $-7.33$  ( $\beta$ -VO<sub>2</sub>) eV, respectively.<sup>46,48</sup> A comparison of these results with those for V<sub>2</sub>O<sub>5</sub> obtained from DFT ( $-16.41$  eV)<sup>49</sup> and experimental determination ( $-16.07$  eV)<sup>46</sup> shows that the PW91 functional overestimates the stability of the more oxygen-rich vanadia phases compared to that of the reduced ones.

Figure 3 shows that the thinnest ( $1 \times 1$ ) O=V-terminated film ( $\sim 2$  Å, 1V layer) is stable for chemical potentials of V and O that are not sufficient (not high enough) for the formation of bulk V<sub>2</sub>O<sub>3</sub> oxide, that is, in the region above the dotted line. For the highest chemical potentials, the corresponding thickest possible 6V-layer film forms. There is only a small range of oxygen and vanadium potentials for which 5V-layer films are stable, namely, ( $1 \times 1$ ) O=V (5V layers) and O<sub>3</sub>-V<sub>3</sub>-O<sub>3</sub> (Figure 1E). In an intermediate range, the  $\sqrt{3}$ -(O=V)<sub>1/3</sub> and  $\sqrt{3}$ -(O=V)<sub>2/3</sub> terminations, which result from the ( $1 \times 1$ ) O=V 6V-layer film by partial removal of surface O=V groups and subsequent reconstruction, become stable. Hence, for the thicker films, we find the same possible terminations as those recently predicted for the single-crystal V<sub>2</sub>O<sub>3</sub>(0001) surface.<sup>25</sup> Only six terminations show up, and five of them contain surface vanadyl groups. It is noteworthy that no other intermediate slab thicknesses between the thinnest and thickest ones are stable. The  $\sim 2$ – $6$  Å range corresponds to that of the model catalyst studies of ref 10. Furthermore, a thicker slab (number of trilayers  $> 6$ ), allowing thicker vanadia films, would result in the same surface phase diagram with respect to the stability regions of thin vs thick films. That is, the stability regions for the thicker films in Figure 3 will be replaced by those of even thicker films. Hence, the same surface structures will be present for the latter.

The model catalysts of ref 10 were prepared at room temperature (300 K) under UHV ( $10^{-13}$  atm) conditions, whereas typical reducing conditions correspond to UHV and elevated temperatures (e.g., 800 K). The corresponding  $\Delta\mu_{\text{O}}$  values are approximately  $-0.66$  and  $-1.88$  eV, respectively. In UHV, at 300 K, the calculations favor (mostly) vanadyl-terminated surfaces independent of the film thickness, which is consistent with the analysis of the IR spectra of the vanadia particles in ref 10. The phase diagram indicates that O=V groups are stable up to at least 800 K, which, in turn, is consistent with the results of ref 16.

For a given oxygen pressure and temperature, the precise surface structure depends on the vanadium chemical potential. Depending on the temperature,  $a_{\text{V}}$  values in different ranges will correspond to a given  $\Delta\mu_{\text{V}}$  value. For large  $\Delta\mu_{\text{V}}$  values (high vanadium activity), the ( $1 \times 1$ ) O=V-covered, 6V-layer surface is the stable phase. As the V percentage decreases, the reconstructed  $\sqrt{3}$ -(O=V) <sub>$x$</sub>  phases with  $x = 2/3$  and, in turn,  $1/3$  become more favorable.

The values of  $\Delta\mu_{\text{V}}$  for which these transitions occur are approximately 1 eV smaller in UHV at 300 K than those obtained at 800 K. These terminations have less vanadyl groups and are more vanadium-poor (more oxygen-rich) compared to the ( $1 \times 1$ ) O=V phase. For even lower  $\Delta\mu_{\text{V}}$  values in UHV at 300 K, the vanadyl groups are unstable, and the whole surface reconstructs, yielding a O<sub>3</sub>-V<sub>3</sub>-O<sub>3</sub> termination and no vanadyl groups. This VO<sub>2</sub> termination is also stable at 800 K but at higher O<sub>2</sub> pressure ( $\sim 1$  atm). For  $\Delta\mu_{\text{V}} < 1/2[\Delta E^{\text{V}_2\text{O}_3} - 3\Delta\mu_{\text{O}}]$ , that is, values above the dotted line in Figure 3, the ultrathin films (1V layer) stabilize at the ( $1 \times 1$ ) O=V termination. At 300 K and UHV, a  $\Delta\mu_{\text{V}}$  value approximately 2 eV lower than that at 800 K is required to stabilize this 1V-layer film. Upon further reduction of  $\Delta\mu_{\text{V}}$ , the thin films should become unstable, and the stability of small vanadia particles (e.g., V<sub>2</sub>O<sub>5</sub> clusters)

on the Al<sub>2</sub>O<sub>3</sub> surface should be favored. This study is deferred to an accompanying paper.<sup>50</sup>

Our calculations suggest that the termination of V <sub>$n$</sub> O <sub>$m$</sub>  films ( $\geq 6$  Å) grown on alumina may be varied either by changing the temperature at a given O<sub>2</sub> pressure (V supply switched off) or by varying the vanadium activity while controlling  $T$  and the oxygen pressure. If UHV and room temperature are assumed, for instance, *four* terminations are possible at varying values of  $\Delta\mu_{\text{V}}$ . These structures are likely to be present among the thick particles ( $\sim 5$ – $6$  Å) grown on alumina at these conditions.<sup>10</sup> Thus, the presence of vanadyl species, as observed in the IR spectra, does not necessarily imply a complete coverage with O=V groups ( $1 \times 1$  termination).

As mentioned above, at 300 K, a partial pressure of approximately  $10^{-13}$  atm corresponds to  $\Delta\mu_{\text{O}} \approx -0.66$  eV, which is not significantly different from the values that correspond to conditions typically employed in oxidation reactions, namely, atmospheric pressure and a temperature of 500–600 K ( $\Delta\mu_{\text{O}} = -0.50$  and  $-0.61$  eV, respectively). Thus, the results of the present study suggest that the discussed stable terminations are expected to also exist at catalytically relevant conditions.

Finally, it is important to mention that the PW91 functional tends to overestimate formation and binding energies, which means that the calculated chemical potentials may shift by several hundred millielectronvolts. Thus, the absolute pressures and activities may change by 2–3 orders of magnitude. Moreover, the overestimation of the stability of the more oxygen-rich bulk vanadia phases mentioned above also applies to the theoretically predicted stability ranges of the  $\sqrt{3}$ -(O=V) <sub>$x$</sub>  terminations of the supported films. Theory puts the subsequent transitions between the ( $1 \times 1$ ) O=V,  $\sqrt{3}$ -(O=V)<sub>2/3</sub>, and  $\sqrt{3}$ -(O=V)<sub>1/3</sub> terminations at somewhat lower (i.e., more negative)  $\Delta\mu_{\text{O}}$  values. This was recently shown for the V<sub>2</sub>O<sub>3</sub>(0001) surface, for which theory<sup>25</sup> and experiment<sup>22</sup> agree that O=V groups are progressively removed from the surface with increasing oxygen pressure; however, they disagree on the range in which the ( $1 \times 1$ ) O=V and  $\sqrt{3}$ -(O=V) <sub>$x$</sub>  terminations are stable.

**B. Vanadyl-Terminated versus Metal-Terminated Films.** Removal of all vanadyl oxygen atoms from the ( $1 \times 1$ ) O=V-terminated films results in a fully reduced film that is single-metal terminated. Statistical thermodynamics tells us that, in UHV, O=V groups are stable up to temperatures of 800 K (cf. section III.A). The reason is the large reaction energy for this process, which is defined as

$$E_{\text{r}} = E_{\text{V}} - E_{\text{O=V}} + \frac{1}{2}E_{\text{O}_2} \quad (13)$$

in which  $E_{\text{V}}$  and  $E_{\text{O=V}}$  are the total energies of the ( $1 \times 1$ ) cell of a fully reduced (metal-terminated) slab and the corresponding completely O=V-covered surface slab, respectively. Figure 4 shows  $E_{\text{r}}$  as a function of film thickness, with  $n$  being the number of V layers in the film ( $n = 1$ – $6$ , 12). For  $n = 6$ ,  $E_{\text{V}}$  and  $E_{\text{O=V}}$  refer to the slabs shown in Figure 1A and 1D, respectively.

For the thinnest 1V-layer film ( $n = 1$ ), the largest value is obtained (4.27 eV/atom). Gradually increasing the thickness of the V<sub>2</sub>O<sub>3</sub> film leads to energy oscillations with decreasing amplitude. The lowest value corresponds to the 2V-layer film with the sequence (V–O<sub>3</sub>–V)–(Al–O<sub>3</sub>–Al); that is, it contains a V–Al double-metal layer at the V<sub>2</sub>O<sub>3</sub>/Al<sub>2</sub>O<sub>3</sub> interface. For a 3V-layer film, (V–O<sub>3</sub>–V)(V–O<sub>3</sub>–Al), a value of 4.11 eV/atom

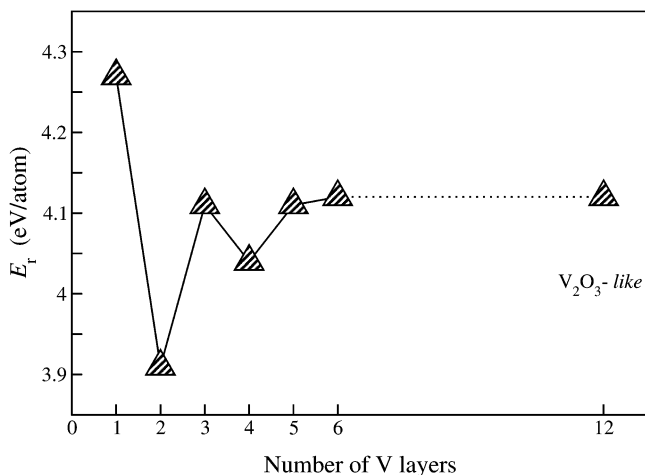


**Figure 4.** Reaction energy  $E_r$  in eV/atom as a function of the number of V layers for  $(1 \times 1)$  O=V-terminated thin vanadia films on  $\alpha$ -Al<sub>2</sub>O<sub>3</sub>.

is obtained, which differs from that of the V<sub>2</sub>O<sub>3</sub>-like surface ( $n = 12$ ) by only 0.2%. The  $\sim 4\%$  in-plane lattice mismatch between the V<sub>2</sub>O<sub>3</sub> and  $\alpha$ -Al<sub>2</sub>O<sub>3</sub>(0001) single-crystal surfaces results in a value for the limiting V<sub>2</sub>O<sub>3</sub>-like case that is 0.07 eV/atom larger than that for the V<sub>2</sub>O<sub>3</sub>(0001) surface. Thus, with respect to the removal of the vanadyl oxygen atoms from all surface vanadyl groups, a 3V-layer film already behaves like the single-crystal V<sub>2</sub>O<sub>3</sub>(0001) surface. However, films of intermediate thickness, such as the 3V-layer film, do not show up in the stability plot.

**C. Vanadyl Oxygen-Induced V<sub>2p</sub> Surface Core-Level Shifts.** As mentioned in the Introduction, surface-sensitive XPS helped solve the apparently conflicting results of ref 10, namely, the observation of a characteristic V=O stretch frequency and vanadium atoms in the oxidation state III. Indeed, for the vanadium atoms at the vanadyl terminated V<sub>2</sub>O<sub>3</sub>(0001) surface, a shift of the V<sub>2p</sub> core levels of  $\sim 2$  eV toward higher binding energies compared to those for the reduced films (i.e., single-metal-terminated) has been observed<sup>16</sup> and confirmed by calculations<sup>25</sup> and additional experiments.<sup>22</sup>

In the following, we examine the V<sub>2p</sub> adlayer core-level shift ( $\Delta_{\text{ACLS}}$ ) for the V atoms in the surface layer induced by the presence of the vanadyl oxygen atoms for differently terminated vanadia films. As mentioned in section III.B, a 3V-layer film behaves like a V<sub>2</sub>O<sub>3</sub>(0001) single-crystal surface with respect to vanadyl oxygen removal. Therefore, we consider the  $(1 \times 1)$  O=V-terminated (metallic) surfaces with three (or more) V layers and the reconstructed  $\sqrt{3}\text{-(O=V)}_x$  structures.

The oxygen-induced V<sub>2p</sub> core-level shift is the difference between the core ionization energy at the vanadyl-terminated surface and that at the reduced one. Using Slater's transition state concept<sup>51,52</sup> to evaluate total energy differences, the total shift ( $\Delta_{\text{ACLS}}$ ) is approximated by

$$\Delta_{\text{ACLS}} \approx -(\epsilon_{0.5}^{\text{vanadyl}} - \epsilon_{0.5}^{\text{reduced}}) \quad (14)$$

This shift is decomposed into an initial state contribution,  $\Delta_{\text{ACLS}}^{\text{initial}}$  and a screening contribution,  $\Delta_{\text{screening}}$ :

$$\Delta_{\text{ACLS}}^{\text{initial}} = -(\epsilon^{\text{vanadyl}} - \epsilon^{\text{reduced}}) \quad (15)$$

The values  $\epsilon^{\text{vanadyl}}$  and  $\epsilon^{\text{reduced}}$  are the Kohn–Sham eigenvalues of the V<sub>2p</sub> core-states of a V atom at the O=V-terminated and reduced surfaces, respectively. The values  $\epsilon_{0.5}^{\text{vanadyl}}$  and  $\epsilon_{0.5}^{\text{reduced}}$  are the corresponding eigenvalues after the removal of half of

an electron from the 2p states. The eigenvalues refer to the Fermi level. The considered systems have a Fermi reservoir of electrons. Thus, to describe the transition state, spin-polarized, self-consistent calculations using a modified PAW potential were performed under the constraint of charge neutrality. This implies that half of a valence electron was added at the Fermi level. By generation of the core-excited PAW potentials, half of a core electron is excited. The other core electrons are not allowed to relax, whereas the screening by the valence electrons is included. The impurity problem of the localized core-hole is treated using the supercell approach. For the smallest  $(1 \times 1)$  cell, atoms with core-holes are separated by  $\sim 4.8$  Å.

Table 2 shows the vanadyl-induced V<sub>2p</sub> core-level shift and its initial and screening contributions for the 3V-layer  $(1 \times 1)$  O=V-terminated supported film. Values are given for the atom of the surface layer (V<sub>1</sub>), to which oxygen is directly bonded, and average values are given for the atoms in the second and third layers (V<sub>2</sub> and V<sub>3</sub>). DFT predicts that, in the outermost V layer (V<sub>1</sub>), V<sub>2p</sub> core electrons are, by 1.53 eV, more bound for the vanadyl-terminated surface than for the single-metal-terminated surface. However, a much smaller shift is predicted for the atoms of the double V-layer beneath. Since screening is small, this is basically an initial state effect. Increasing the film thickness from three to, for example, five V layers results in a 0.19 eV larger shift for the V<sub>1</sub> atoms. For the limiting V<sub>2</sub>O<sub>3</sub>-like case, the value is 1.65 eV.

Figure 5 displays the contribution of the d-states on the vanadium atoms (in the outermost metal layers) to the total density of states (DOS) for the vanadyl-terminated (Figure 5A.1, B.1) and reduced (panels A.2 and B.2) films. A and B refer to the 1V- and 3V-layer films, respectively. Figure 5C.1, C.2 shows the difference between the spin-up and spin-down DOS for the surface V sites (V<sub>1</sub>) for the vanadyl-terminated and reduced 3V-layer films. The integration of these curves (up to the Fermi level) yields 0.03 (O=V) and 1.91 (reduced) electrons, which reflects the vanadyl-induced change in the oxidation state of the surface atoms. The positive initial-state contribution to the shift is due to the increase in the oxidation state of vanadium from V<sup>III</sup> to V<sup>V</sup> on oxygen adsorption leading to O=V bond formation. The gain of local charge at the reduced V sites makes the electrostatic potential repulsive and core-level binding energies decrease. The more efficient screening of the core-hole by intraatomic polarization at the reduced surface correlates with the higher d-DOS of the V<sub>1</sub> atom about the Fermi level.

The value of 1.53 eV calculated for a 3V-layer film differs only by 0.13 eV from that calculated for the single-crystal V<sub>2</sub>O<sub>3</sub>(0001) surface atoms (see Table 2). The latter compares well with the experimentally observed shift of  $\sim 2$  eV (ref 16). A non-spin-polarized calculation for the V<sub>2</sub>O<sub>3</sub>(0001) surface (ref 25) yields only 0.91 eV. Using the LDA+U method, the calculated shift is 1.86 eV.<sup>25</sup> For the reconstructed  $\sqrt{3}\text{-(O=V)}_x$  terminations, we find similar vanadyl oxygen-induced V<sub>2p</sub> shifts, namely, 1.73 and 1.69 eV for  $x = 1/3$  and  $2/3$ , respectively. In the experimental work of ref 22, no difference between the measured V<sub>2p</sub> shift of vanadyl-terminated sites at different structures is reported. Our calculated small differences support this observation.

**D. Formation of Vanadyl Oxygen Defects.** In view of the above-mentioned relation between the catalytic performance of supported vanadia catalysts and surface reducibility, we examine first the dissociation of the O=V surface bonds of the unreconstructed vanadyl-terminated 1V- and 6V-layer (Figure 1D) films. The results are (vanadyl) oxygen defects, and we

**TABLE 2: Oxygen-Induced  $V_{2p}$  Adlayer Core-Level Shifts and Their Initial-State and Screening Contributions (in eV) for the Three Outermost V Layers of the 3V-Layer-Supported  $V_2O_3$  Film and the  $V_2O_3(0001)$  Surface**

	3V-layer-supported $V_2O_3$ film			$V_2O_3(0001)^b$			$V_2O_3(0001)^c$
	$\Delta_{\text{ACLS}}$	$\Delta_{\text{ACLS}}^{\text{initial}}$	$\Delta_{\text{screening}}$	$\Delta_{\text{ACLS}}$	$\Delta_{\text{ACLS}}^{\text{initial}}$	$\Delta_{\text{screening}}$	$\Delta_{\text{ACLS}}$
$V_1$	1.53	1.34	0.19	1.66	1.20	0.46	0.91
$V_2-V_3^a$	0.18	0.38	-0.20	0.09	0.19	-0.10	0.12

<sup>a</sup> Average of the shifts for the V atoms in the second and third V layers. <sup>b</sup> This work: spin-polarized calc. <sup>c</sup> Ref 25: non-spin-polarized calc.

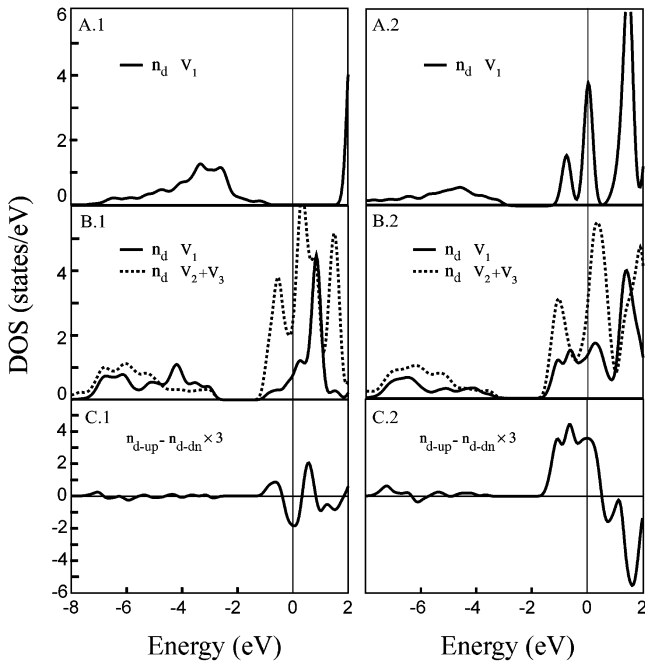


**Figure 5.** d-orbital-projected DOS,  $n_d$ , for the V atoms in the outermost metal layers. A and B refer to the 1V- and 3V-layer films, respectively. Full lines correspond to the topmost V layer, whereas the dotted lines to the sum of the V atoms in the double-metal layer beneath. A.1/B.1/C.1 and A.2/B.2/C.2 refer to the  $(1 \times 1)$  O=V and the reduced single-metal terminations, respectively. The d-orbital projected spin density,  $(n_{d\text{-up}} - n_{d\text{-dn}})$  for the  $V_1$  atom of the 3V-layer films are shown in C.1/C.2 panels. The curves are smoothed by a Gaussian level broadening of 0.2 eV. The energy zero is at the Fermi level.

consider different defect concentrations  $\Theta_{\text{def}} = N_{\text{def}}/N_{\text{tot}}$ . The values  $N_{\text{def}}$  and  $N_{\text{tot}}$  are the actual and maximum possible number of vanadyl oxygen defects in the unit cell, respectively.

The average vacancy formation energy,  $E_f(\Theta_{\text{def}})$  is given by

$$E_f(\Theta_{\text{def}}) = E_{\text{red}}(\Theta_{\text{def}}) - E_{\text{O=V}} + N_{\text{def}} \frac{1}{2} E_{\text{O}_2} \quad (16)$$

in which  $E_{\text{red}}(\Theta_{\text{def}})$  represents the total energy of the reduced surface slab. (Note that this equation reduces to eq 13 for  $\Theta_{\text{def}} = 1$ , i.e., a fully reduced surface.)

Using eq 16, we calculate the energy required to create defect structures with  $\Theta_{\text{def}} = 1/4, 1/3, 1/2, 2/3, 3/4$ , and 1 employing  $(2 \times 2)$  and  $(\sqrt{3} \times \sqrt{3})R30^\circ$  unit cells. The creation of an isolated oxygen defect at the fully O=V-terminated surfaces corresponds to  $\Theta_{\text{def}} = 1/4$  and  $1/3$  for the respective surface cells. The energy cost for the consecutive removal of such defects is given by

$$\Delta E_f(\Theta_{\text{def}}) = \begin{cases} E_f(\Theta_{\text{def}}) - E_f\left(\Theta_{\text{def}} - \frac{1}{4}\right) & \Theta_{\text{def}} = 1/4, 1/2, 3/4, \text{ and } 1 \\ E_f(\Theta_{\text{def}}) - E_f\left(\Theta_{\text{def}} - \frac{1}{3}\right) & \Theta_{\text{def}} = 1/3 \text{ and } 2/3 \end{cases} \quad (17)$$

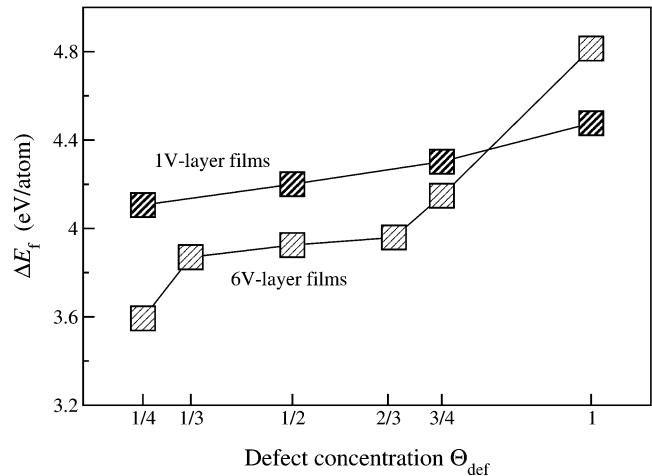


**Figure 6.** Calculated vanadyl oxygen vacancy formation energies in eV/atom for a single defect as a function of the defect concentration  $\Theta_{\text{def}}$  for 1V- and 6V-layer films ( $\Delta E_f(\Theta_{\text{def}})$ ; see eq 17).

For example,  $\Delta E_f(\Theta_{\text{def}} = 1/2)$  is the energy for removal of a second vanadyl oxygen from a  $(2 \times 2)$  surface cell.

Figure 6 shows the results for the ultrathin 1V- and the thick 6V-layer films. For both films, it is easiest to create the first defect. Thus, the formation of additional defects becomes more difficult with increasing defect concentration,  $\Theta_{\text{def}}$ . Furthermore, the calculations suggest a somewhat *less* facile reduction of the ultrathin 1V-layer film. For instance, the creation of a single defect ( $\Theta_{\text{def}} = 1/4$ ) for the 1V-layer film (4.11 eV) is by  $\sim 0.5$  eV more costly than that for the 6V-layer film (3.59 eV). This may relate to the insulating nature of the vanadyl-terminated 1V-layer system (see Figure 5A). Moreover, the  $\Theta_{\text{def}}$  dependence due to repulsive interactions is less pronounced for this thin film (0.37 eV between  $\Theta_{\text{def}} = 1/4$  and 1).

For other film terminations that are likely to be stable, namely, the  $\sqrt{3}\text{-}(\text{O=V})_x$  phases, the energy cost to remove a single vanadyl oxygen is 3.75 eV for  $x = 2/3$  and 3.90 eV for  $x = 1/3$ . These values lie between the  $\Delta E_f(\Theta_{\text{def}} = 1/4)$  for the 6V-layer (3.59 eV) and 1V-layer (4.11 eV)  $(1 \times 1)$  O=V films. It is noteworthy that this sequence of defect formation energies follows exactly the order of stable terminations in the calculated phase diagram, as the oxygen pressure decreases while the vanadium chemical potential is kept constant (see Figure 3 for the example of  $\Delta\mu_{\text{V}} \approx -2.5$  eV). Phases that are stable at low oxygen pressure are those that most strongly resist oxygen release (or defect formation) into the gas phase, whereas phases that easily release oxygen require high oxygen pressure for stabilization.

In summary, oxygen-defect formation at stable surfaces of supported vanadium oxide films requires between 4.11 and 3.59 eV per  $1/2\text{O}_2$  molecule, which is much larger than the 1.93 eV found for the  $V_2O_5(001)$  surface.<sup>49</sup> The reason is the following: on the supported films, defect formation converts a O=V<sup>V</sup>( $d^0$ ) site into a V<sup>III</sup>( $d^2$ ) one, and the structure relaxation effects are small (e.g., less than 0.1 eV for 1V-layer film and  $\Theta_{\text{def}} = 1/$

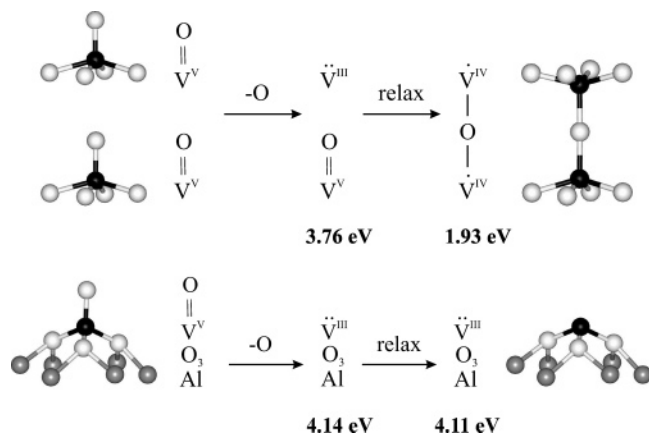


**Figure 7.** Schematic representation of the oxygen-induced structure and electronic effects at the  $V_2O_5(001)$  single-crystal (upper part) and the 1V-layer ( $1 \times 1$ ) O=V film supported on  $\alpha\text{-Al}_2\text{O}_3(0001)$  surface (lower part). The defect formation energies correspond to those for single defects.

4). In contrast, oxygen defect formation at the  $V_2O_5(001)$  single-crystal surface is accompanied by a large relaxation, which leads to the formation of a V–O–V bond, with the  $V_2O_5$  layer beneath the surface layer, and converts the  $V^{III}(d^2)$  site (initially formed upon reduction) into a more stable pair of  $V^{IV}(d^1)$  sites (see Figure 7). Consequently, the defect formation energy is lowered from 3.76 to 1.93 eV.<sup>49</sup> The value for  $V_2O_5(001)$  without relaxation is within the range of values obtained for the supported films in this work. The possibility of such relaxations yielding to bond formation is due to the layered structure of the crystalline  $V_2O_5(001)$ , and it does not exist in the corundum structure of the supported films. This provides a possible explanation for the lower catalytic activity in selective oxidation reactions of vanadium oxides supported on alumina compared to that of the crystalline  $V_2O_5$  particles.<sup>3,4</sup>

#### IV. Summary and Conclusions

We have presented a detailed study of  $\sim 2\text{--}6$  Å thick vanadia films supported on  $\alpha$ -alumina, combining DFT and statistical thermodynamics. The calculated phase diagram suggests that, at room temperature and UHV, ( $1 \times 1$ ) O=V-terminated ultrathin films (thickness  $\sim 2$  Å) are stable for low vanadium activities. As the vanadium activity increases, films can become as thick as the vanadium supply allows, and different surface structures are possible, namely, a reconstructed oxygen-terminated ( $O_3\text{--}V_3\text{--}O_3$ ) surface, two partially covered by O=V groups, exhibiting a  $(\sqrt{3} \times \sqrt{3})R30^\circ$  geometry, and an unreconstructed surface exclusively terminated by O=V groups. These terminations were also predicted to be stable for the  $V_2O_3(0001)$  single-crystal surface.<sup>25</sup> Moreover, all of them are likely to be present not only in UHV at 300 K but also at catalytically relevant conditions (1 atm,  $\sim 500\text{--}600$  K).

For both supported films and  $V_2O_3(0001)$  surfaces, a shift of about 2 eV for the  $V_{2p}$  core levels of the surface vanadium atoms indicates the existence of terminating vanadyl oxygen atoms. However, observation of this shift does not necessarily imply complete coverage with O=V groups ( $1 \times 1$  termination). The phase diagram shows that surface vanadyl groups are stable up to at least 800 K in UHV.

If we accept that the catalytic activity of a vanadia catalyst depends on its reducibility, the energy of oxygen defect formation may be used as an indicator of its catalytic performance. Reducing a  $V^V(d^0)$  site to a  $V^{III}(d^2)$  site on ultrathin ( $1 \times 1$ ) O=V-terminated film costs approximately 4.1 eV per

$1/2O_2$ . For the other stable alumina-supported vanadia films, the defect formation energy varies between 4.1 and 3.6 eV. In contrast, reduction of the  $V_2O_5(001)$  single-crystal surface that yields a pair of  $V^{IV}(d^1)$  centers costs only about half of this amount (1.9 eV). This relates to the observed lower activity in oxidation reactions of vanadium oxides when supported on alumina.

#### V. Acknowledgments

This work was supported by Deutsche Forschungsgemeinschaft (Sonderforschungsbereich 546). T.K.T. thanks the Fonds der Chemischen Industrie for a fellowship. We thank G. Kresse for helpful comments on the VASP code and V. Brázdová and A. Hofmann for useful discussions. The calculations were carried out on the IBM p690 system of the Norddeutscher Verbund für Hoch- und Höchstleistungsrechnen (HLRN). We would like to thank B. Kallies for technical support.

**Supporting Information Available:** Table of total energies and surface related free energies for all systems studied. This material is available free of charge via the Internet at <http://pubs.acs.org>.

#### References and Notes

- (1) Chen, K.; Iglesia, E.; Bell, A. T. *J. Catal.* **2000**, *192*, 197.
- (2) Argyle, M. D.; Chen, K.; Resini, C.; Krebs, C.; Bell, A. T.; Iglesia, E. *J. Phys. Chem. B* **2004**, *108*, 2345.
- (3) Wachs, I. *Catal. Today* **2005**, *100*, 79.
- (4) Weckhuysen, B. M.; Keller, D. E. *Catal. Today* **2003**, *78*, 25 and references therein.
- (5) Guo, Q.; Lee, S.; Goodman, D. W. *Surf. Sci.* **1999**, *437*, 38.
- (6) Wand, Q.; Madix, R. J. *Surf. Sci.* **2001**, *474*, L213.
- (7) Chang, Z.; Piligkos, S.; Möller, P. *J. Phys. Rev. B* **2001**, *64*, 165410.
- (8) Calatayud, M.; Mguig, B.; Minot, C. *Surf. Sci. Rep.* **2004**, *55*, 169.
- (9) Vittadini, A.; Selloni, A. *J. Phys. Chem. B* **2004**, *108*, 7337.
- (10) Magg, N.; Giorgi, J.; Schroeder, T.; Bäumer, M.; Freund, H.-J. *J. Phys. Chem. B* **2002**, *106*, 8756.
- (11) Magg, N.; Giorgi, J.; Hammoudeh, A.; Schroeder, T.; Bäumer, M.; Freund, H.-J. *J. Phys. Chem. B* **2003**, *107*, 9003.
- (12) Magg, N.; Immaraporn, B.; Giorgi, J.; Schroeder, T.; Bäumer, M.; Döbler, J.; Wu, Z.; Kondratenko, E.; Cherian, M.; Baerns, M.; Stair, P. C.; Sauer, J.; Freund, H.-J. *J. Catal.* **2004**, *226*, 88.
- (13) Brázdová, V.; Ganduglia-Pirovano, M. V.; Sauer, J. *Phys. Rev. B* **2004**, *69*, 165420.
- (14) Wu, Z.; Kim, H.-S.; Stair, P. C.; Rugmini, S.; Jackson, S. D. *J. Phys. Chem. B* **2005**, *109*, 2793.
- (15) Keller, D. E.; de Groot, F. M. F.; Koningsberger, D. C.; Weckhuysen, B. M. *J. Phys. Chem. B* **2005**, *109*, 10223.
- (16) Dupuis, A.-C.; Hajja, M. A.; Richter, B.; Kühlenbeck, H.; Freund, H.-J. *Surf. Sci.* **2003**, *539*, 99.
- (17) Surnev, S.; Vitali, L.; Ramsey, M. G.; Netzer, F. P.; Kresse, G.; Hafner, J. *Phys. Rev. B* **2000**, *61*, 13945.
- (18) Surnev, S.; Kresse, G.; Ramsey, M. G.; Netzer, F. P. *Phys. Rev. Lett.* **2001**, *87*, 086102.
- (19) Kresse, G.; Surnev, S.; Ramsey, M. G.; Netzer, F. P. *Surf. Sci.* **2001**, *492*, 329.
- (20) Surnev, S.; Ramsey, M. G.; Netzer, F. P. *Prog. Surf. Sci.* **2003**, *73*, 117.
- (21) Schoiswohl, J.; Sock, M.; Eck, S.; Surnev, S.; Ramsey, M. G.; Netzer, F. P.; Kresse, G. *Phys. Rev. B* **2004**, *69*, 155403.
- (22) Schoiswohl, J.; Sock, M.; Surnev, S.; Ramsey, M. G.; Netzer, F. P.; Kresse, G.; Andersen, J. N. *Surf. Sci.* **2004**, *555*, 101.
- (23) Niehus, H.; Blum, R.-P.; Ahlbehrendt, D. *Phys. Status Solidi A* **2001**, *187*, 151.
- (24) Niehus, H.; Blum, R.-P.; Ahlbehrendt, D. *Surf. Rev. Lett.* **2003**, *10*, 353.
- (25) Kresse, G.; Surnev, S.; Schoiswohl, J.; Netzer, F. P. *Surf. Sci.* **2004**, *555*, 118.
- (26) Kresse, G.; Hafner, J. *Phys. Rev. B* **1993**, *48*, 13115.
- (27) Kresse, G.; Furthmüller, J. *Comput. Mater. Sci.* **1996**, *6*, 15.
- (28) Kresse, G.; Furthmüller, J. *J. Phys. Rev. B* **1996**, *54*, 11169.
- (29) The version VASP 4.4.5, released on November 26, 2001, was used.
- (30) Perdew, J. P.; Chevary, J. A.; Vosko, S. H.; Jackson, K. A.; Pederson, M. R.; Singh, D. J.; Fiolhais, C. *Phys. Rev. B* **1992**, *46*, 6671.
- (31) Blöchl, P. E. *Phys. Rev. B* **1994**, *50*, 17953.

- (32) Kresse, G.; Joubert, D. *Phys. Rev. B* **1999**, *59*, 1758.
- (33) Monkhorst, H. J.; Pack, J. D. *Phys. Rev. B* **1976**, *13*, 5188.
- (34) Manassidis, I.; Vita, A. De; Gillan, M. J. *Surf. Sci.* **1993**, *285*, L517.
- (35) Wang, X.-G.; Chaka, A.; Scheffler, M. *Phys. Rev. Lett.* **2000**, *84*, 3650.
- (36) Verdozzi, C.; Jennison, D. R.; Schultz, P. A.; Sears, M. P. *Phys. Rev. Lett.* **1999**, *82*, 799.
- (37) Herzberg, G. *Molecular Spectra and Molecular Structure. I. Spectra of Diatomic Molecules*, 2nd ed.; Robert E. Krieger Publishing Co., Inc.: Malabar, FL, 1989.
- (38) Perdew, J. P.; Burke, K.; Ernzerhof, M. *Phys. Rev. Lett.* **1996**, *77*, 3865.
- (39) Zhang, Y.; Yang, W. *Phys. Rev. Lett.* **1998**, *80*, 890.
- (40) Sauer, J.; Döbler, J. *Dalton Trans.* **2004**, *19*, 3116.
- (41) Czekaj, I.; Hermann, K.; Witko, M. *Surf. Sci.* **2003**, *545*, 85.
- (42) Zhang, S. B.; Northrup, J. E. *Phys. Rev. Lett.* **1991**, *67*, 2339.
- (43) Zhang, W.; Smith, J. R.; Wang, X.-G. *Phys. Rev. B* **2004**, *70*, 024103.
- (44) Stull, D. R.; Prophet, H., Eds.; *JANAF Thermochemical Tables*, 2nd ed.; U.S. National Bureau of Standards: Washington, DC, 1971.
- (45) Wagman, D. D.; Evans, W. H.; Parker, V. B.; Schumm, R. H.; Halow, I.; Bailey, S. M.; Churney, K. L.; Nuttall, R. L. *J. Phys. Chem. Ref. Data* **1982**, *11*, Supplement 2.
- (46) Linstrom, P. J., Mallard, W. G., Eds. *NIST Chemistry WebBook*; National Institute of Standards and Technology: Gaithersburg, MD, 2001 (<http://webbook.nist.gov>).
- (47) Kubaschewski, O., Alcock, C. B., Spencer, P. J., Eds. *Materials Thermochemistry*, 6th ed.; Pergamon Press: Oxford, 1993.
- (48) Brückner, W., Oppermann, H., Reichelt, W., Terukow, J. I., Tschudnowski, F. A., Wolf, E., Eds. *Vanadiumoxide Darstellung, Eigenschaften, Anwendung*; Akademie-Verlag: Berlin, 1983.
- (49) Ganduglia-Pirovano, M. V.; Sauer, J. *Phys. Rev. B* **2004**, *70*, 045422.
- (50) Brázdová, V.; Ganduglia-Pirovano, M. V.; Sauer, J. *J. Phys. Chem. B* **2005**, *109*, 23532.
- (51) Slater, J. C. In *Quantum Theory of Molecules and Solids*; McGraw-Hill: New York, 1974; Vol. 4.
- (52) Janak, J. F. *Phys. Rev. B* **1978**, *18*, 7165.
- (53) Kirfel, A.; Eichhorn, K. *Acta Crystallogr.* **1990**, *A46*, 271.
- (54) Dernier, P. D. *J. Phys. Chem. Solids* **1970**, *31*, 2569.